JOURNAL OF CATALYSIS 140, 526–542 (1993)

Comparison between Zeolite β and γ-Al_2O_3 Supported Pt for Reforming Reactions

PANAGIOTIS G. SMIRNIOTIS AND ELI RUCKENSTEIN[1]

Department of Chemical Engineering, State University of New York at Buffalo, Buffalo, New York 14260

Received July 7, 1992; revised November 12, 1992

The performance of zeolite β supported platinum as a bifunctional catalyst for the reforming of *n*-hexane, methylcyclopentane, and cyclohexane, typical representatives of reforming feeds, has been examined under low severity conditions. A comparison under the same conditions with γ-Al_2O_3 supported Pt was carried out. Both catalysts were impregnated with 0.5 wt% Pt. It is found that β-zeolite exhibits skeletal isomerization reactions to a higher extent than alumina, producing molecules with much higher octane number than the feed molecules. Bimolecular alkylation reactions that take place in the zeolite pores have as a result the formation of products with a carbon number larger than that of the feed molecule. The enlargement of the cyclic ring of methylcyclopentane leads at suitable temperatures to aromatics, a reaction of great importance for reforming. This behavior is a result of the relatively large acidity of the zeolite and of its pore structure that favors the proximity among different molecules increasing the probability for reaction. In contrast, Pt/Al_2O_3 stimulates dehydrogenation–hydrogenation and to a smaller extent skeletal isomerization. The β-zeolite is deactivated more easily than alumina due to the coke build up on the acidic sites. The characterization of the catalysts has been carried out using XRD, NH_3-TPD, SEM, FTIR, BET, TEM, and H_2-Chemisorption. © 1993 Academic Press, Inc.

INTRODUCTION

It is well known that high-silica-content zeolites are attractive catalysts for many industrial processes because of their hydrothermal and acidic stability, high resistance to coking, and high activity and selectivity for specific types of reactions (*1*). The β-zeolite, which was first synthesized by Wadlinger *et al.* (*2*), belongs to this class since it can possess a SiO_2/Al_2O_3 ratio in the range of 5 to 100 (*3*). Its structural characteristics have been investigated recently by Newsam *et al.* (*4*) and Treacy and Newsam (*5*). They found that zeolite β possesses a three-dimensional 12-ring pore system and that its structure is a highly faulted intergrowth of two distinct, but closely related structures: polymorph A (tetragonal) and polymorph B (monoclinic). Thus, the β-zeolite is a combination of the polymorph A structure, which has straight channels of 0.73 × 0.60 nm and tortuous channels of 0.56 × 0.56 nm, and polymorph B, which has straight channels of 0.73 × 0.68 nm and tortuous channels of 0.55 × 0.55 nm. Because of its pore opening, zeolite β can accommodate molecules with diameters larger than those which can be accommodated by ZSM-5, and can provide shape selectivity for intermediate size molecules to a higher extent than X and Y faujasites. Very recently a second monoclinic polymorph C of zeolite β has been reported by Higgins *et al.*(*6*).

The crystallization rate of the β-zeolite and its crystal size depend strongly on the total alkali content and the relative proportion of Na^+ and K^+ cations (*7*). Studies of the crystallization process of zeolite β have been carried out by Perez-Pariente *et al.* (*8*, *9*). The zeolite crystallinity is altered significantly by the water to alumina and the template to alumina molar ratios. It was also

[1] To whom correspondence should be addressed.

0021-9517/93 $5.00
Copyright © 1993 by Academic Press, Inc.
All rights of reproduction in any form reserved.

found that a very crystalline zeolite can be obtained after two weeks at 160°C by using tetraethylammonium hydroxide (TEAOH) as template, if the H_2O/Al_2O_3 molar ratio is kept below 600 (*10*). For high crystallinity, the molar ratio $TEAOH/Al_2O_3$ has to be above 2.

There are only a few papers in the literature on the catalytic behavior of zeolite β, since it has been relatively disregarded after its initial synthesis in 1967. Zeolite β has beneficial effects in the catalytic hydrodewaxing of petroleum oils by lowering their pour point (*11–13*). The catalytic activity of Pt/H-β zeolite has been examined by Martens *et al.* (*14*) for the isomerization and hydrocracking of long chain paraffins. They found that metal-supported β-zeolite behaves as an ideal bifunctional catalyst that exhibits high activity for primary cracking and selectivity for isomerization. The activity of H-β zeolite for cracking of gas-oil has been compared to that of HY zeolite (*15*). It was found that zeolite β is less active and produces less gasoline and more coke than HY zeolite. For the cracking of *n*-heptane it was observed that zeolite β exhibits a slightly higher activity than HY zeolite and lower hydrogen transfer capability (*16*). The reactions of aromatic hydrocarbons, such as the methylation and disproportionation of toluene and the isomerization of *m*-xylene over Pt/β zeolite, have been also investigated (*17*). It was found that because of its relatively large pores, it does not provide any product shape selectivity for the isomerization of *m*-xylene to *o*- and *p*-xylenes, but in contrast to the 10-membered ring pores zeolites such as ZSM-5 which has smaller pores, it favors the disproportionation reactions. On the other hand it suppresses the formation of the larger trimethylbenzene molecules. The disproportionation and transalkylation of toluene and trimethylbenzene over β-zeolite have been also examined (*18*). It was found that β-zeolite exhibits excellent catalytic stability and transalkylation selectivity.

In the present work the performance of β-zeolite and γ-Al_2O_3, both impregnated with Pt, for the reforming reaction of *n*-hexane, methylcyclopentane, and cyclohexane is examined. All reactants have six carbon atoms, and constitute typical representatives of reforming feeds. However, as it was noted by Weisz (*19*), Ciapetta and Wallace (*20*), and Ramage *et al.* (*21*), they follow different mechanisms of reaction. Low severity operating conditions (relatively low temperatures and atmospheric total pressure) have been chosen in order to minimize possible hydrocracking (*22*).

The zeolite β stimulates the skeletal isomerization of *n*-hexane to a higher extent than alumina, producing even dibranched hexanes. This is a result of the increased ability of β-zeolite for isomerization over its acidic sites of the olefinic intermediates which are generated on the metal. Its ability for production of aromatics by dehydrocyclization is also higher than that of Al_2O_3, probably because of the geometrical constraint imposed by its pore structure. A small degree of hydrocracking of *n*-hexane was found to occur in the zeolite. Zeolite β transforms methylcyclopentane to dibranched molecules with a cyclic ring of six carbon atoms and dibranched aromatic molecules to a much greater extent than Al_2O_3. These products, which have higher octane number than the feed molecule, are a result of: (1) the stimulation of bimolecular alkylation reactions between cycloolefinic intermediates generated by the dehydrogenation of the feed molecules over the Pt sites, with carbonium ions produced by the ring opening of other feed molecules over the acidic sites of the zeolite, and (2) the disproportionation of the alkylated intermediate molecules formed. The reactions of cyclohexane show that Al_2O_3 has a higher ability for dehydrogenation-hydrogenation than β-zeolite, probably because of the higher Pt dispersion. Instead, the zeolite possesses a significantly higher ability for the isomerization of cyclohexane. The rate of deactivation of β-zeolite is higher than that of alumina because of some coke build up on the acidic sites.

EXPERIMENTAL

Synthesis and Preparation of the Catalyst

Zeolite β has been synthesized hydrothermally from an aluminosilicate gel with the nominal composition 3TEAOH–30 SiO_2–Al_2O_3–0.9Na_2O–250H_2O containing tetraethylammonium hydroxide (TEAOH) as template. The reagents used were: colloidal silica (LUDOX HS-40, Du Pont) containing 40 wt% SiO_2 and 0.41 wt% Na_2O; sodium aluminate (Fisher Scientific); tetraethylammonium hydroxide (Aldrich 40 wt% solution in water); sodium chloride (Fisher Scientific); and distilled water. Individual solutions of the above chemicals were mixed with vigorous stirring for 45 min in the appropriate proportions. The pH of the resultant gel was 13. The gel was loaded in a Teflon lined stainless-steel autoclave (Autoclave Engineers) and kept at 160 ± 1°C under autogeneous pressure for 10 days without stirring. At the end of the crystallization period the autoclave was quenched in cold water and the zeolite was separated by filtering the content of the autoclave and washing the precipitate thoroughly with distilled water. After drying the resulting zeolite overnight at 140°C it was found that a high yield, 97 wt% of the solid material originally used for the gel preparation, has been achieved.

The protonated form of the zeolite has been prepared as follows: TEAOH-β samples were heated at 500 ± 2°C for 5 h by increasing the temperature at a rate of 10°C/min in an ultra high purity O_2 flow (5 ml/min) in order to burn the template occluded in the pores of the zeolite. At this calcination temperature, the structure of the zeolite is preserved unchanged, as found by Perez-Pariente *et al.* (*23*) and Liu *et al.* (*24*). The zeolite was exchanged with 2M ammonium sulfate (Fisher) for 4 h at 90 ± 1°C. The remaining sodium after the cation exchange was 0.021 wt% while the molar ratio of SiO_2/Al_2O_3 was 23. A second calcination at 450°C for 1 h has followed. High purity γ-Al_2O_3 (PURALOX SB a-230) was kindly donated to us by Condea Chemie GmbH. The sample had a surface area of 228 m^2/g, and a Na_2O content below 0.005 wt%. The preparation of the platinum-loaded catalysts has been carried out by impregnation with H_2PtCl_6 (Aldrich 8 wt% solution in water). The Pt loading was 0.5 wt% for both catalysts (estimated on a dry basis). After impregnation the catalysts were dried overnight at 130°C.

X-ray Diffraction and Infrared Spectroscopy

The X-ray diffraction spectra of zeolite β were obtained with a Nicolet powder X-ray diffractometer equipped with a CuK_α source. For the quantification of its crystallinity we followed the procedure described by Yarlagada *et al.* (*25*). Samples made with various proportions of high crystallinity β-zeolite having a molar ratio of SiO_2/Al_2O_3 = 25 (PQ Corporation, CP 811 BL-25), were mixed thoroughly with MgO (Baker analyzed 99.6 wt%). The ratio of the area under the two more intense peaks of the reference β-zeolite ($2\theta \simeq 7.8°$ and $2\theta \simeq 22.6°$) to the area under the main peak of MgO vs the weight percentage of β-zeolite was employed as the calibration curve. Calcined samples of the prepared β-zeolite mixed with MgO in various proportions were compared with the calibration curve to determine the extent of their crystallinity.

For the infrared investigation of the zeolite, a Fourier transform-infrared spectrometer (Mattson Alpha Centauri) has been used. Transmittance spectra have been obtained in the range of 4000–400 cm^{-1} with a resolution of 4 cm^{-1}. Prior to the actual run, thin wafers of the zeolite (1 wt%) in KBr have been prepared in a dry atmosphere under a pressure of 56 atm.

NH_3-TPD Experiments

For the determination of the acidity of the catalysts, NH_3 temperature-programmed desorption has been employed. A sample of 0.2 g H-β zeolite or γ-Al_2O_3 was heated for 1 h at 400°C in high purity helium in order to remove possible impurities and moisture

from the sample. The bed was heated at a rate of 10° C/min. After the bed was cooled down, pulses of anhydrous ammonia (Matheson) were introduced into the bed until complete saturation (T = 25°C) of the catalyst was achieved. After the adsorption step, the bed was flushed with helium for 1 h at T = 25°C. The temperature-programmed desorption took place in the range of 25 to 700°C with a heating rate of 10°C/min and a carrier gas flow of He of 20 ± 0.5 cm^3/min. The detection of the desorbed ammonia has been made with a tungsten-rhenium thermal conductivity detector of a Perkin–Elmer (Sigma 2000) gas chromatograph. The dead volume from the bed to the detector has been kept minimal in order to increase the accuracy. A mixture of liquid nitrogen and heptanol has been used as a trap after the bed in order to collect any possible moisture removed from the zeolite pores or produced by the hydroxyl groups of alumina at high temperatures.

H_2-Chemisorption

Hydrogen chemisorption has been employed for the determination of the metal dispersion. After calcination and reduction, the catalysts were loaded in a pyrex-glass sample holder located in a furnace of a vacuum glass system equipped with a pressure transducer. A reduction in flowing H_2 at 200°C for 1 h has followed in order to eliminate the possible partial oxidation of the catalysts during their transfer to the glass holder. The samples were evacuated at 10^{-5} Torr and 400°C for 1 h and then cooled down to room temperature (T = 24°C) under the same vacuum. High purity H_2 was introduced at pressures between 10 to 400 Torr for the determination of the total amount (irreversible and reversible) of H_2 adsorbed. After this step, the samples were evacuated at 10^{-5} Torr and room temperature for the elimination of the weakly bound H_2, and a second adsorption curve at room temperature over the latter samples regarding the weakly bound hydrogen was determined. The amount of strongly chemisorbed H_2 was obtained after subtracting the two isotherms and extrapolating the results to zero pressure. The metal dispersion was evaluated assuming that H/Pt is 1 : 1.

Catalytic Runs

The catalytic experiments were conducted in a plug flow differential reactor operating at 1 atm pressure. Prior to the reaction, the catalysts were activated by oxidation in situ in the reactor by flowing 5 ± 0.5 ml/min ultra high purity oxygen (99.999%) at 400°C for 2 h. In all the experiments the reactor was heated at a rate of 10°C/min. After this step, a purging of the catalyst with high purity He (99.995%) for 15 min, followed by its reduction in flowing 5 ± 0.5 ml/min ultra high purity H_2 (99.999%) at 400°C for 2 h, brought the catalysts to their final state for reaction. Hydrogen, at a predetermined flow rate, was bubbled through a bubbler containing the appropriate hydrocarbon to be fed into the reactor, at 24°C. The composition of the feed stream was found to be independent of the flow rate through the bubbler, indicating that the stream is saturated with the feed molecules. The reactants were *n*-hexane (Aldrich 99 + wt%), methylcyclopentane (Aldrich 98 wt%) and cyclohexane (anhydrous Aldrich 99 + wt%). With these compounds the H_2/Oil molar ratios were 4.4, 4.8, and 7.4, respectively.

In all the catalytic runs, 100 ± 2 mg (on a dry basis) of catalyst were loaded on a glass wool plug located at the middle of a vertical stainless steel tube reactor $\frac{1}{8}$ in. in diameter. High-resolution gas chromatography has been used for the on-line analysis of the effluent stream. The analysis was carried out with a gas chromatograph (Hewlett-Packard 5890 Series II) associated with a Mass Spectrometer (Hewlett-Packard 5971). The chromatograph was loaded with a Poraplot capillary column (ID 0.53 mm, length 28 m with a film thickness of 20 μm), a molecular sieve packed column (5A) and a high performance capillary column (HP-1, ID 0.2 mm, length 12 m, with a film thickness of 0.33 μm).

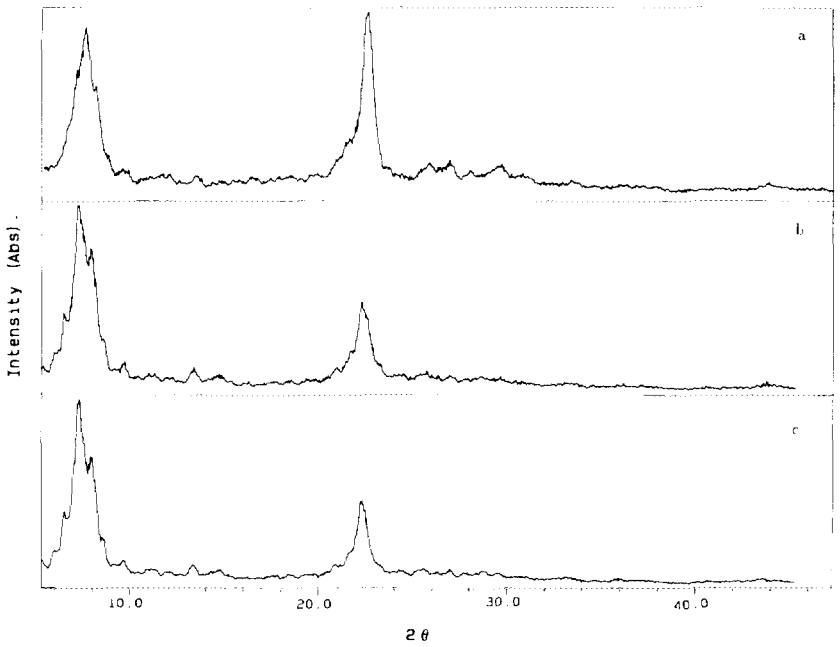

FIG. 1. X-ray diffraction pattern of β-zeolite (a) as produced, (b) calcined at 550°C in O_2 for 5 h, and (c) after four calcinations at 550°C in O_2 for 5 h each.

RESULTS AND DISCUSSION

X-ray

The X-ray diffraction pattern of the β-zeolite matched closely with that published earlier (*26*). It was found that the synthesized zeolite is highly crystalline, what is expected because of the relatively high SiO_2/Al_2O_3 ratio in the initial gel (*9*). A comparison of the X-ray pattern of the prepared β zeolite with those computed as a function of fault probability by Newsam *et al.* (*4*) indicated the existence of almost equal amounts of polymorphs A and B. The decrease of the height of the peak at $2\theta \simeq 22.6°$ after calcination, shown in Fig. 1, is probably due to microstructural defects that are introduced (*15*). Additional four successive calcinations of the zeolite at 550°C for 5 h each, led to negligible decreases in the height of this peak. The morphology of the zeolite crystals was examined with a scanning electron microscope (Hitachi S-800). They have spherical shape with an average diameter of about 1 μm.

BET Measurements

The effect of calcination time and temperature on the surface area of zeolite β is given in Table 1. The measurements have been carried out with a surface area, pore volume analyzer (Model 2100D Micromeritics), after degassing the samples overnight at

TABLE 1

Surface Area of Zeolite β as a Function of Calcination Conditions

T_C(°C)	t_C(h)[a]	S_g(m²/g)
Uncalcined[b]	—	79.3
500	5	400.3
500	12	398.6
600	5	387.5
600	12	277.0

[a] T_C = calcination temperature, t_C = calcination time.

[b] For the uncalcined zeolite the degassing was carried out at 200°C to avoid the contamination of the BET apparatus with the unburned template.

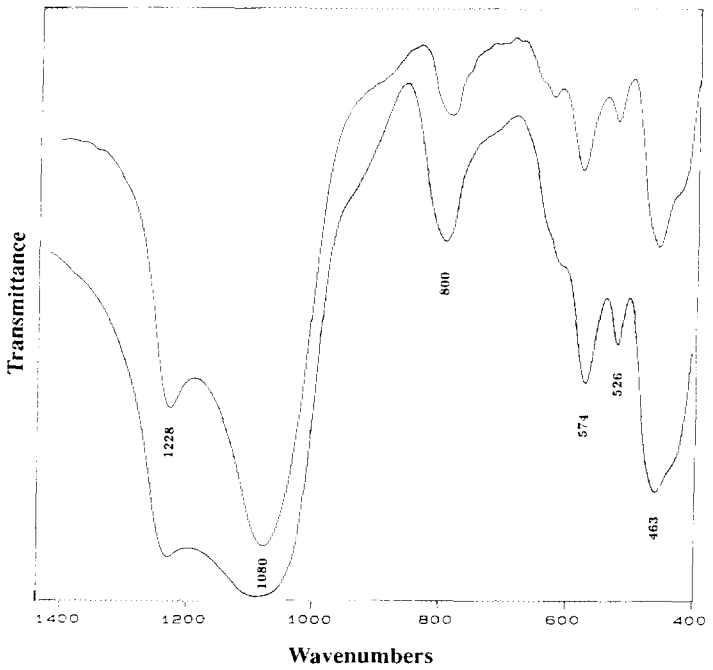

FIG. 2. Mid-Infrared spectra of β-zeolite (the top curve is for calcination at T_C = 600°C for 5 h, the bottom curve is for calcination at T_C = 500°C for 5 h).

350°C. One can note a relatively large decrease of the surface area after long calcination at high temperatures (above 600°C). The small value of S_g for the uncalcined sample is probably due to the unburned template.

Infrared Spectroscopy

The identification of the prepared powder as the β-zeolite is also supported by its mid-infrared spectrum given in Fig. 2, where the characteristic peak of β at 526 cm^{-1} appears (*9, 26*). The complete burning of the template during calcination has been achieved since no peaks were found which can be assigned to the ethyl groups of the template (3100–2800 cm^{-1} for stretching vibrations and 1500–1300 cm^{-1} for bending vibrations). By examining the region of the asymmetric stretching vibrations, which is between 1250 and 950 cm^{-1} (*27*), one can observe a decrease of the peak height at 1228 cm^{-1} with increasing calcination temperature. The relative decrease of the height of this peak indicates a crystallographic change in the structure of the zeolite at high temperatures (above 600°C). The peak at 1080 cm^{-1} is insensitive to the heat treatment, like all the peaks which are due to internal tetrahedra (*27*). In the range of symmetric stretching vibrations (950–650 cm^{-1}), there is a main peak at 800 cm^{-1} which can be assigned to the external linkages of AlO_4 tetrahedra vibrations. Its height decreases with increasing calcination temperature, indicating a crystallographic change. The peaks at 574 cm^{-1} and 526 cm^{-1} (the latter is specific to zeolite β only) are in the range of the double ring vibrations of tetrahedra, while the one at 463 cm^{-1} can be assigned to TO_4 bending vibrations of the internal tetrahedra. The additional peak at 526 cm^{-1}exhibited by the β-zeolite results probably from the double four ring (D4R) vibrations of β, since its framework contains a large fraction of 4-membered rings (*4, 6*). On the other hand,

TABLE 2

Platinum Dispersion D (=H/Pt) of Pt/Zeolite β and Pt/γ-Al_2O_3

	T_O(°C)	T_R(°C)[a]	D = H/Pt
γ-Alumina	400	400	0.60
β-Zeolite	300	300	0.23
β-Zeolite	400	400	0.06

Note. For both catalysts the metal loading is 0.5 wt%. The duration of oxidation and reduction was 2 h each.

[a] T_O = oxidation temperature, T_R = reduction temperature.

calculations (*28*) show that the infrared vibrations for D4R occur around 630, 539, and 527 cm^{-1}, while for D6R, around 605, 584, and 510 cm^{-1}. Pentasil zeolites, such as the ZSM-5 do not possess such peaks since its framework consists exclusively of five-membered rings (*29, 30*).

NH_3-TPD

The NH_3-TPD spectrum of β-zeolite matched well with those presented in the earlier work of Hedge *et al.* (*31*). An intense low temperature peak appears due to the weakly bounded ammonia on silanol groups. However, the acidity of β-zeolite is correlated with another less intense peak that appears in the region of 400°C. This peak was found to be very broad and is shifted to lower temperatures compared to that of ZSM-5 (500–550°C), indicating the stronger acidity (*32*) of the latter catalyst. The spectrum of γ-Al_2O_3 shows a less intense peak than that of zeolite β. Alumina possesses (*33*) Lewis acidity which is produced after the water removal during heating at high temperatures (*34*), and a much lower Brønsted acidity.

H_2-Chemisorption

As results from Table 2, the dispersion of Pt is higher on γ-Al_2O_3 than on the zeolite. Transmission electron micrographs (JEOL-100 CX operating at 100 KV) barely show Pt particles located on the surface of γ-Al_2O_3 (Fig. 3a), indicating that a large fraction of Pt is well dispersed. Under the present oxidation and reduction conditions (400°C for 2 h), the metal dispersion over the zeolite β is significantly lower than that on Al_2O_3. Figure 3b shows a large number of Pt particles (around 50 Å) located on the external surface of the zeolite crystals. The oxidation and reduction of the zeolite under less severe conditions, namely 300°C for 2 h (not given), showed fewer Pt particles located on the zeolite crystal surface. Of course, the metal dispersion is higher in this case. A similar behavior was observed earlier (*35*) with Pt over NaY zeolite oxidized and reduced at higher temperatures. Originally, during the calcination step, Pt^{2+} ions are transferred to the sodalite cages. During the reduction step, the Pt^0 atoms formed migrate from the sodalite cages, through the zeolite channels, to the external surface of the zeolite. As a result, the availability of Pt inside the zeolite pores is reduced. The chloride concentrations in both catalysts under different oxidation-reduction conditions are given in Table 3. The catalysts were dissolved in HNO_3 and the Cl^- concentration was measured potentiometrically with a selective ion chloride probe.

Catalytic Behavior

n-Hexane. The product distribution of γ-Al_2O_3 given in Table 4 shows negligible hydrocracking of *n*-hexane, due to its small Brønsted acidity. As a result, the production of C_1, C_2 molecules is very low. The (moderate) acidity of β-zeolite is expected to favor mainly the skeletal isomerization of the olefinic intermediates formed on Pt sites. This is confirmed by the product distribution given in Table 5. The probabilities for primary and secondary cracking are small, otherwise the ratios C_1/C_5 and C_2/C_4 would be even larger than unity (*36, 37*). This is supported by the fact that at elevated temperatures, up to 400°C, only small amounts of C_1, C_2 hydrocarbons are formed. The generation of propane, which increases with in-

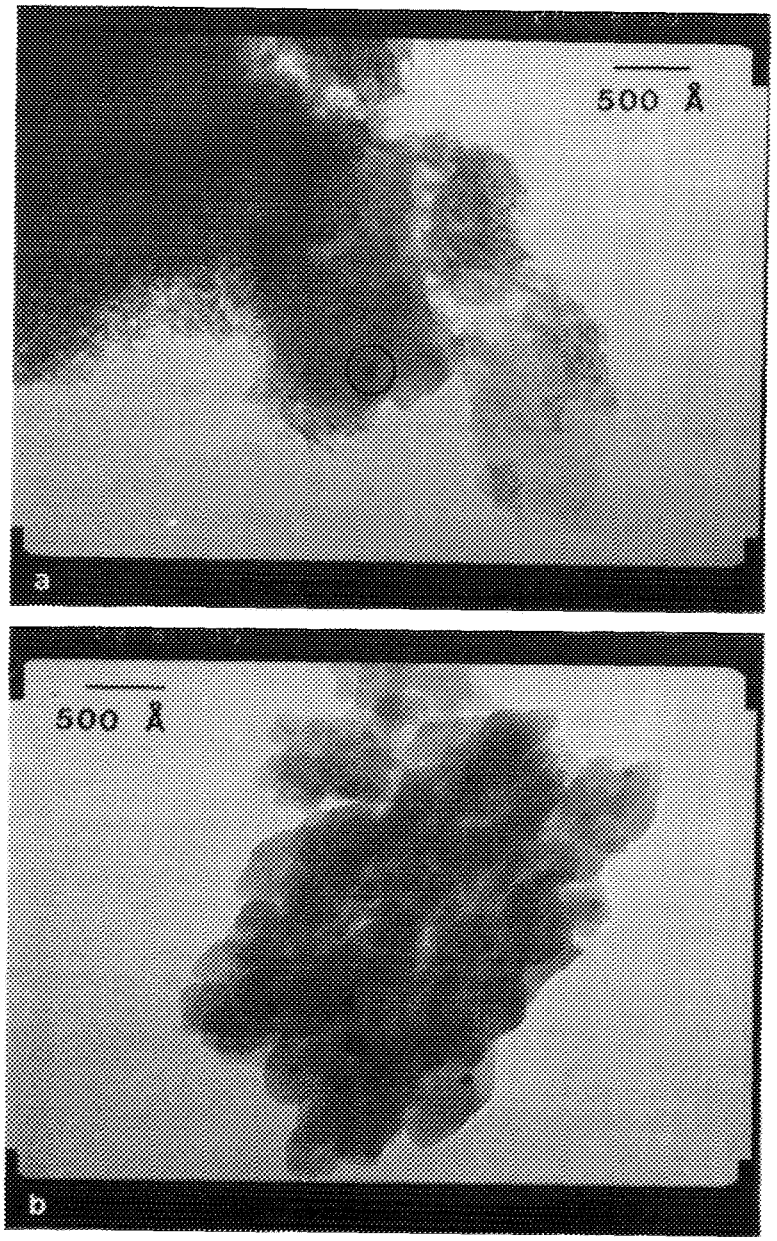

FIG. 3. (a) Transmission electron micrograph of Pt/γ-Al_2O_3 calcined at 400°C for 2 h and reduced at 400°C for 2 h and (b) transmission electron micrograph of Pt/β zeolite calcined at 400°C for 2 h and reduced at 400 C for 2 h.

creasing temperature, can be partially attributed to a multistep hydrocracking (*19*) consisting of the dehydrogenation of hexane to 3-hexene, followed by the "center cracking" of hexene to C_3 olefins on the acid sites, and finally by the hydrogenation of the latter molecules over Pt sites to propane. The production of linear and branched C_4, C_5 hydro-

TABLE 3

Chloride Concentration of β-Zeolite and γ-Al_2O_3 under Different Oxidation Reduction Conditions

	T_O(°C)	T_R(°C)[a]	Cl (mg/g cat.)
β-Zeolite	As impregnated		3.53
β-Zeolite	Calculated[a]		2.59
β-Zeolite	300	300	2.75
β-Zeolite	400	400	1.63
β-Zeolite	550	550	0.82
γ-Alumina	As impregnated		3.44
γ-Alumina	400	400	5.07

[a] The calculation is based on the fact that both catalysts were impregnated with H_2PtCl_6 for a metal loading of 0.5 wt%.

carbons cannot be a result of the direct cracking of *n*-hexane via the β-scission of a C_6 cation, since as already mentioned, C_1 and C_2 are present in small amounts compared to C_4 and C_5 hydrocarbons. Their generation probably takes place via the alkylation reactions of C_6 molecules with olefinic molecules having less than six carbon atoms. This bimolecular reaction is stimulated by the appropriate size of the β-zeolite pores. A subsequent cracking of the $C_{>6}$ cations thus produced, can explain the C_3–C_5 hydrocarbon yields. Olefins have not been detected as final products in the present experiments probably because of their hydrogenation over Pt. A similar behavior has been observed earlier by Poutsma and Schaffer (*38*) with *n*-hexane over REY and $RE(NH_4)Y$ (rare earth faujasit). They suggest that the origin of C_4 and C_5 products from a C_6 precursor is not a result of direct cracking, but a result of the alkylation of an olefinic intermediate that generates a molecule with more than six carbon atoms, followed by cracking. The branched C_4 and C_5 hydrocarbons which are produced in relatively large amounts by zeolite β (Table 4), have significantly larger octane numbers than *n*-hexane (*39*, *40*).

The zeolite promotes skeletal isomerization to a much higher extent than γ-Al_2O_3 (compare Table 4 with column 2 of Table 5). It generates even dibranched C_6 molecules, while γ-Al_2O_3 does not possess such a capability. Alumina produces from *n*-hexane mainly 2-methyl and 3-methylpentane, by the isomerization mechanism of linear paraffins known to occur over bifunctional nonzeolitic catalysts (*19*, *20*). According to this mechanism, the dehydrogenation of the paraffin over the metal (Pt) results in an olefinic intermediate which is further isomerized on the acidic sites to produce a monobranched intermediate. In the final step, the hydrogenation of the branched intermediate over Pt generates a monobranched paraffin. The isomerization step of the olefin is the rate-controlling step, since independent experiments with both *n*-pentane and 1-pentene have shown the same isomerization rate (*41*). The same mechanism can be applied to the formation of monobranched isomers of *n*-hexane over the Pt loaded β zeolite.

TABLE 4

Product Distribution from *n*-Hexane (WHSV = 1.95 h^{-1}), Methylcyclopentane (WHSV = 1.76 h^{-1}), and Cyclohexane (WHSV = 1.22 h^{-1}) over Pt-Supported γ-Al_2O_3 after 1 h on Stream at 300°C

Products	mole%
n-Hexane WHSV = 1.95 h^{-1}	
Propane	0.1
Butane	0.1
n-Pentane	0.2
2-Methylpentane	8.4
3-Methylpentane	6.2
n-Hexane	85.0
Methylcyclopentane WHSV = 1.76 h^{-1}	
Propane	0.1
n-Pentane	0.6
2-Methylpentane	4.2
3-Methylpentane	2.0
Methylcyclopentane	87.0
Benzene	5.9
Toluene	0.2
Cyclohexane WHSV = 1.22 h^{-1}	
Propane	0.7
Methylcyclopentane	0.1
Benzene	92.8
Cyclohexane	2.2
Toluene	4.2

TABLE 5

Product Distribution from *n*-Hexane against WHSV over Pt-Supported Zeolite β after 1 h on Stream at $T = 300°C$

Products (mole%)	WHSV (h^{-1})					
	0.47	1.95	3.55	6.51	8.97	11.71
Methane	0.4	0.3	0.3	0.8	0.4	0.4
Ethane	0.4	0.1	0.5	0.8	0.3	0.2
Propane	12.0	10.3	9.6	11.2	3.5	2.4
i-Butane	23.0	10.6	9.3	5.1	5.6	4.5
n-Butane	6.4	2.7	3.4	2.6	1.6	1.0
i-Pentane	14.3	7.0	6.6	3.6	3.2	2.3
n-Pentane	6.1	4.8	3.6	2.3	1.3	1.0
2,2-Dimethylbutane	5.1	5.0	5.3	1.2	2.7	2.6
2,3-Dimethylbutane	2.3	4.3	4.1	3.5	4.2	4.6
2-Methylpentane	12.3	20.1	22.5	26.2	27.0	27.5
3-Methylpentane	9.9	19.6	20.6	18.6	20.9	22.3
n-Hexane	7.7	15.2	14.2	23.7	28.8	31.2

The suitable size of the zeolite pores can in addition stimulate the transformation of a part of the monobranched olefinic intermediates into dibranched ones by bond shift of carbon atoms. The hydrogenation over Pt of the dibranched olefinic intermediate produces dibranched paraffins. This behavior is probably a combined result of the acidity (both Brønsted and Lewis (*16*)) of the zeolite and of its pore structure, which enables different carbon atoms of the same molecule to be brought closer. As suggested by Martens *et al.* (*42*), high isomerization yields can be achieved if the dehydrogenation-hydrogenation function and the Brønsted acidity of the bifunctional catalyst are in balance. The isomerization yields of a well-balanced bifunctional zeolite depends strongly on the carbon number of the *n*-paraffin and on the pore size of the zeolite. The lower isomerization of Al_2O_3 is due to its lower acidity while no dibranching occurs probably because of its larger pores.

To explain the production of dibranched hexane molecules in Y zeolite, Bolton and Lanewala (*37*) proposed the existence of a bimolecular transition state intermediate generated through the close adsorption of two hexane molecules on the catalyst surface. The final product distribution of the hexane isomers is a result of the disproportionation reactions of different transition states of the two *n*-hexane molecules. These bimolecular transition states cannot be completely excluded for zeolite β, but they occur to a much smaller extent than with Y zeolite and probably only in the straight channels of β which are comparable in size with those of Y.

The ratio of the products 2-methylpentane/3-methylpentane (2-MP/3-MP) is higher than unity for both Al_2O_3 and β zeolite catalysts under all conditions (*37*). This indicates that the equilibrium between the methylpentanes is shifted towards 2-methylpentane. A cyclic reaction mechanism which involves a methylcyclopentane intermediate was also suggested to explain the isomerization of *n*-hexane (*43*). This mechanism does not seem to occur in either of the two catalysts employed in the present study, since the C_6 isomers generated from *n*-hexane and methylcyclopentane are different (compare Tables 5 and 6).

The effect of the temperature on the conversion of *n*-hexane over β zeolite and γ-Al_2O_3 is presented in Figs. 4, 5, respectively. Zeolite β has a much higher activity than Al_2O_3. The activity of zeolite β increases with temperature and reaches a pla-

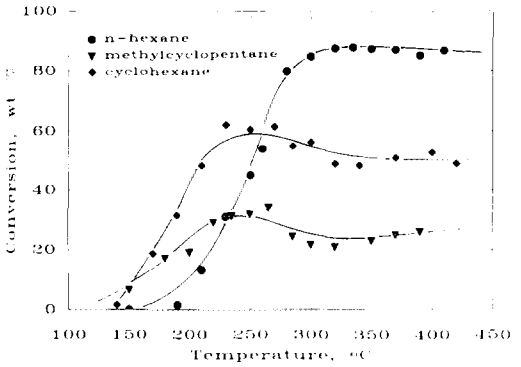

FIG. 4. Conversion vs temperature for the three feeds over β-zeolite (after 1 h on stream, WHSV = 1.95 h^{-1} for *n*-hexane, WHSV = 1.76 h^{-1} for methylcyclopentane, and WHSV = 1.22 h^{-1} for cyclohexane).

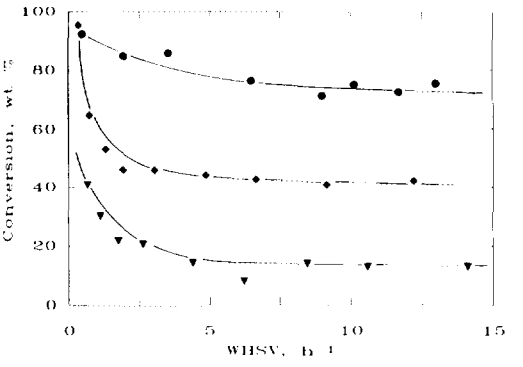

FIG. 6. Conversion vs WHSV for the three feeds over β-zeolite (after 1h on stream at T = 300°C, (●) for *n*-hexane, (▼) for methylcyclopentane, and (◆) for cyclohexane).

teau. Small amounts of toluene and xylenes are produced at high temperatures. The increase of the temperature decreases the yield of the C_6 isomers and increases those of the C_1–C_5 alkanes. Under the same operating conditions, alumina did not produce any aromatics. The pores of the zeolite promote to a higher extent than those of Al_2O_3 branching and some cyclization probably because of their higher acidity and because their size can stimulate the bending around of the linear C_6 molecules.

The effect of the WHSV on the conversion of both catalysts is presented in Figs. 6 and 7. The conversion over Al_2O_3 is relatively low and falls to very small values with increasing WHSV. The product distribution of alumina as a function of the residence time remains relatively unchanged. The conversion over the zeolite is relatively large at small values of WHSV and decreases moderately for high values of WHSV. For the zeolite, the decrease of the residence time reduces the concentrations of C_4, C_5 alkanes but increases those of the C_6 isomers. This indicates that the direct isomerization of the C_6 olefinic intermediate to methylpentanes is faster than its bimolec-

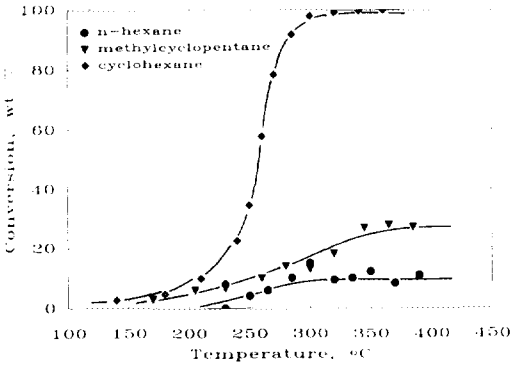

FIG. 5. Conversion vs temperature for the three feeds over γ-Al_2O_3 (after 1 h on stream, WHSV = 1.95 h^{-1} for *n*-hexane, WHSV = 1.76 h^{-1} for methylcyclopentane, and WHSV = 1.22 h^{-1} for cyclohexane).

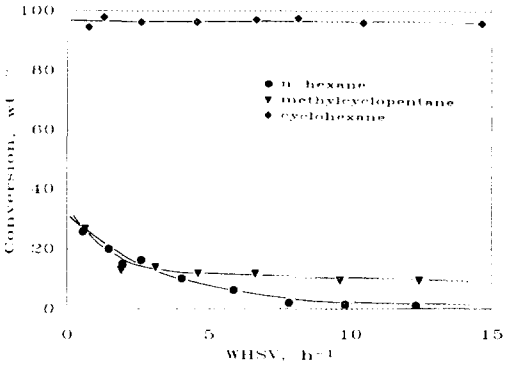

FIG. 7. Conversion vs WHSV for the three feeds over γ-Al_2O_3 (after 1 h on stream at T= 300°C).

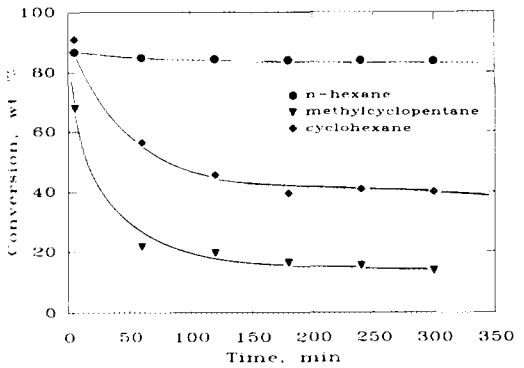

FIG. 8. Conversion vs temperature for the three feeds over β-zeolite (after 1 h on stream at T = 300°C, WHSV = 1.95 h^{-1} for *n*-hexane, WHSV = 1.76 h^{-1} for methylcyclopentane, and WHSV = 1.22 h^{-1} for cyclohexane).

ular reaction with smaller molecules or with itself which lead to larger molecules whose rupturing generates C_3–C_5 alkanes.

The effect of the deactivation of both catalysts as a function of time on stream at 300°C is presented in Figs. 8 and 9 for the zeolite and the Al_2O_3, respectively. Low deactivation is observed for both catalysts, probably because of the small amounts of aromatic or cyclic intermediates, mainly methylcyclopentane (*44*), formed which are precursors for coke formation. At higher temperatures the activity decreases faster, particularly for the zeolite because of coke formation.

Methylcyclopentane. The production distributions for both catalysts under the same operating conditions are given in Tables 4 and 6. As suggested earlier (*19*, *40*), the reforming of alkylcyclopentanes on Al_2O_3 obeys the following mechanism: (a) dehydrogenation of the methylpentane to methylpentene over Pt; (b) some hydrogenolysis over the metal sites resulting in small amounts of small molecular weight hydrocarbons, and mainly isomerization of methylcyclopentene to cyclohexene over the acidic sites via a carbenium ion mechanism; and finally (c) dehydrogenation of cyclohexene to benzene over Pt. The above mechanism explains the generation of aromatics and hydrocracked molecules. The opening of the cyclopentane ring can also occur and generates hexane isomers. This mechanism is indeed followed by Al_2O_3 in the present experiments (Table 4). The absence of cyclohexane indicates that alumina favors the dehydrogenation over the Pt sites of the intermediate cyclohexene molecules generated over its acidic sites.

The above reaction scheme cannot explain completely the product distribution of the zeolite (Table 6) which contains relatively large yields of C_4, C_5, and of aromatic hydrocarbons with larger number of carbon atoms than the feed molecule. The very small ratios of C_1/C_5 and C_2/C_4 exclude hydrocracking and hydrogenolysis as main reactions. The C_6 alkanes are produced by the opening of the cyclic ring of methylcyclopentane. If each of the C–C bonds of methylcyclopentane had equal probabilities for rupturing, the product distribution among the hexane isomers would be *n*-Hex. : 2-MP : 3-MP = 2 : 2 : 1. However, deviations from the above distribution exist for both catalysts. *n*-Hexane is not generated by any of the two catalysts, indicating that the probability of opening of the tertiary–secondary C–C bonds is much smaller than the probability of opening of the secondary–secondary C–C bonds (*43*). In addi-

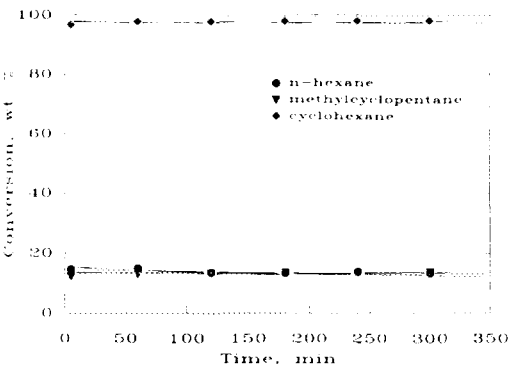

FIG. 9. Conversion vs temperature for the three feeds over γ-Al_2O_3 (after 1 h on stream at T = 300°C, WHSV = 1.95 h^{-1} for *n*-hexane, WHSV = 1.76 h^{-1} for methylcyclopentane, and WHSV = 1.22 h^{-1} for cyclohexane).

TABLE 6

Product Distribution from Methylcyclopentane against WHSV over Pt-Supported Zeolite β after 1 h on Stream at T = 300°C

Products (mole%)	WHSV (h^{-1})				
	0.66	1.76	4.41	6.22	10.57
Ethane	0.2	0.1	—	—	—
Propane	2.3	0.9	0.7	0.7	0.5
i-Butane	6.4	3.5	2.4	2.4	2.1
n-Butane	1.6	0.7	0.5	0.5	0.5
i-Pentane	3.9	2.1	1.3	1.4	1.1
n-Pentane	0.4	0.2	0.1	0.2	0.3
Cyclopentane	1.2	0.4	0.4	0.3	0.4
2-Methylpentane	2.4	1.0	1.0	1.1	0.9
Methylcyclopentane	59.2	78.4	85.7	85.9	87.1
Benzene	3.0	1.6	1.2	0.9	1.9
Cyclohexane	5.8	4.4	2.8	3.1	1.5
1,3-Dimethylcyclopentane	1.7	1.3	0.6	0.6	0.6
Methylcyclohexane	2.6	2.4	1.1	1.0	1.0
Toluene	2.9	0.8	0.8	0.7	0.8
1,4-Dimethylcyclohexane	0.9	1.1	0.3	0.1	0.3
Ethylbenzene	0.5	0.2	0.2	—	—
o-Xylene	0.6	0.1	—	—	—
m-Xylene	1.7	0.4	0.5	0.4	0.4
p-Xylene	0.8	0.2	0.2	0.2	0.2
1,2,3-Trimethylbenzene	1.0	0.1	—	—	—
1-Ethyl-3-methylbenzene	0.5	0.1	0.2	—	—
1-Ethyl-4-methylbenzene	0.4	0.1	—	—	—

tion, for the zeolite the ratio of 2-MP : 3-MP deviates significantly from 2 : 1. Other researchers (*45*) noted a similar deviation. They suggested that the hydrogenolytic splitting of methylcyclopentane on Pt sites proceeds predominantly on the C–C bond of the ring in the β-position to the carbon atom bearing the methyl group. The low dispersion of Pt in the zeolite is probably responsible for the low dehydrogenation of cyclohexene (produced over the acidic sites) to benzene.

It is worth noting that the zeolite produces dibranched aromatic and cyclic molecules with six carbon atoms to a much greater extent than Al_2O_3, particularly at small WHSV. This increases significantly the octane number of the feed molecule, fact which is very important since alkylcyclopentanes constitute a large fraction of the napthenic feed stocks used in reforming industry. As mentioned earlier (*19, 20*), a catalyst that has the ability to increase the carbon number of the C_5 cyclic ring, is extremely valuable. A possible reaction mechanism that explains this behavior of zeolite β is the following: In the first step, the feed molecules are dehydrogenated over the metal to generate C_6-cycloolefins. Bimolecular alkylation reactions between these olefinic intermediates and carbonium ions formed by the ring opening of other feed molecules, produce $C_{>6}$ unstable intermediates. In the final step, the latter intermediates undergo disproportionation reactions which produce C_4, C_5 alkanes and C_8, C_7 cyclic and aromatic hydrocarbons. This mechanism is supported by the fact that approximately equal molar amounts of C_5 and C_7 and of C_4 and C_8 are formed at any

WHSV. Other researchers (*46, 47*) have observed a similar behavior of Pt/Ca-Y faujasite. This bimolecular alkylation reaction is perhaps favored by the suitable size of the pores of β zeolite which provides just enough space for the two molecules to be in close contact, thus increasing the probability for reaction. Such type of reaction is less likely to occur in the large pores of the less active Al_2O_3. The above scheme is favored by high residence times, indicating that the bimolecular alkylation reaction is slow and constitutes the rate-controlling step. This ability of the zeolitic structure to favor bimolecular reactions compared with other acid catalysts was also emphasized by Bolton *et al.* (*48*).

The effect of the temperature on the activity of both catalysts is presented in Figs. 4 and 5. For the zeolite the conversion passes through a maximum, because of the increased rate of deactivation above a certain temperature. Al_2O_3 behaves differently. As already suggested (*49*), hydrogen-deficient hydrocarbon residues, formed by extensive dehydrogenation over the metal sites, cover the metallic surface and have as a result the reduction of the hydrogenation–dehydrogenation capability of the catalyst. In addition, coke can be generated on the acidic sites via the polymerization of the precursors transferred from the metal to the acid sites. This results in maxima (at 350 and 270°C) for the selectivities of aromatics and napthenes, respectively. This is expected to occur to a greater extent in the zeolite because of its higher acidity and more facile blocking of its smaller pores.

The increase of WHSV reduces the reforming ability of both catalysts. This occurs mainly because the isomerization over the acid sites and the bimolecular alkylation reactions are relatively slow. The higher decrease in the zeolite activity can be additionally attributed to its higher rate of coke build up. The behavior of both catalysts as a function of time on stream is presented in Figs. 8 and 9. Alumina exhibits negligible deactivation in contrast to zeolite. The higher acidity of the zeolite favors deactivation, because of the formation of unsaturated polycyclic compounds over its more numerous and stronger acid sites. Higher hydrogen pressures are required to minimize the coke precursors, especially if the temperature is high. Re can be used as a second metal to improve the performance of the catalyst (*20*).

Cyclohexane. From the product distribution of γ-Al_2O_3 (Table 3), one can see that alumina generates almost exclusively benzene above a certain temperature. This reaction involves the dehydrogenation of the feed molecule to a cycloolefin C_6 intermediate, followed by its further dehydrogenation to benzene. This behavior is a combined result of the relatively high Pt dispersion on Al_2O_3 and its low Brønsted acidity. It is worth noting that this reaction has been used for the characterization of the dehydrogenation ability of the reforming catalysts.

Zeolite β has the ability to produce aromatic and cyclic molecules with a larger number of carbon atoms than the feed molecule. The bimolecular alkylation reactions described before followed by disproportionation, result in C_4, C_5 isomers and branched cyclic or aromatic hydrocarbons with a larger number of atoms than the feed molecule. Other researchers (*50*) have noted the occurrence of bimolecular reactions between alkyl carbonium ions and benzene over REX and REY zeolites.

The isomerization of cyclohexene to methylcyclopentene and finally to methylcyclopentane takes place to a great extent since the yield of the latter molecule is relatively large.

The effect of the temperature on the conversion of cyclohexane over the two catalysts is presented in Figs. 4 and 5. For the zeolite, a weak maximum can be observed because deactivation becomes significant after a certain temperature. For the present feed molecule there is a monotonic increase of aromatics and of C_2–C_6 alkanes with temperature while the opposite is true for methylcyclopentane. This indicates that the

TABLE 7

Product Distribution from Cyclohexane against WHSV over Pt-Supported Zeolite β after 1 h on Stream at T = 300°C

Products (mole%)	WHSV (h^{-1})				
	0.34	1.22	3.05	6.66	9.15
Ethane	0.4	0.2	—	—	—
Propane	4.7	1.1	0.6	0.4	0.3
i-Butane	11.8	2.4	2.0	1.1	1.0
n-Butane	3.3	0.8	0.5	0.3	0.3
i-Pentane	6.2	1.2	1.0	0.5	0.5
n-Pentane	1.2	0.4	0.2	0.2	0.2
Cyclopentane	2.6	0.6	0.4	0.3	0.2
2-Methylpentane	2.2	0.6	0.5	0.2	0.2
3-Methylpentane	0.7	—	—	—	—
Methylcyclopentane	22.2	21.1	19.2	19.8	18.1
Benzene	17.8	18.6	18.0	18.5	18.8
Cyclohexane	4.6	46.8	54.1	57.4	59.2
1,3-Dimethylcyclopentane	1.5	0.6	0.6	0.3	0.1
Methylcyclohexane	1.9	1.0	1.2	0.3	0.1
Toluene	7.8	1.8	0.7	0.7	0.6
1,4-Dimethylcyclohexane	2.0	0.5	0.2	—	—
Ethylbenzene	0.7	0.6	0.1	0.1	0.1
o-Xylene	1.2	0.2	0.1	—	—
m-Xylene	3.5	0.8	0.4	0.1	0.2
p-Xylene	1.8	0.4	0.2	—	0.1
1,2,3-Trimethylbenzene	1.0	0.2	—	—	—
1-Ethyl-3-methylbenzene	0.4	0.1	0.1	—	—
1-Ethyl-4-methylbenzene	0.5	—	—	—	—

bimolecular alkylation of cyclohexene followed by the disproportionation of the produced intermediate is favored by an increase of temperature to a larger extent than the simple isomerization of the cyclohexene over the acidic sites. For Al_2O_3, an abrupt increase in conversion takes place at temperatures higher than 250°C mainly because the dehydrogenation of cyclohexane to benzene is accelerated by increasing the temperature.

Regarding the effect of the residence time, one can see (Fig. 7) that the conversion remains almost unchanged for alumina as a function of the WHSV. This is because the production of benzene, which is the main product and takes place on Pt sites, is rapid and does not involve the migration of olefinic intermediates to the acidic sites for isomerization, which is a relatively slow process. For Al_2O_3, which has a lower acidity than the zeolite, the possibility for isomerization is reduced and the change of residence time has an insignificant effect since the dehydrogenation step is fast. This is not however, the case with zeolite β (Fig. 6). The slow isomerization reaction that takes place over its acidic sites and the bimolecular alkylation reactions are affected by the residence time and have as a result the reduction of catalyst activity as WHSV increases. As with the previous feed molecule, the molar amounts of C_5 and C_7 and of C_4 and C_8 are approximately equal (Table 7), validating the existence of the bimolecular alkylation mechanism.

The conversion as a function of time on stream for the zeolite (Fig. 8) shows a decrease which is due to coke formation. However, the activity is higher than when meth-

ylcyclopentane is used as a feed, indicating that the coke build up is higher for feeds with C_5 rings than with those having C_6 rings. This was also noted by Parera *et al.* (*44*). Because of its lower acidity, the time on stream behavior of Al_2O_3 (Fig. 9) shows negligible deactivation, indicating that coke build up on the metal crystallites is small under the present operating conditions since in the reaction of cyclohexane only the metal sites of the catalyst are involved.

CONCLUSIONS

Zeolite β promotes skeletal isomerization reactions that produce mono- and dibranched hexane isomers from *n*-hexane. This behavior can be partially attributed to its acidity which is responsible for the isomerization of olefinic intermediates. On the other hand, its pores have the suitable size to stimulate the C–C bond shift of carbonium ions leading to dibranched isomers, and the bending of paraffinic molecules leading to chain closure.

For methylcyclopentane the acidity and the pore structure of β-zeolite facilitate isomerization and bimolecular alkylation reactions. As a result, molecules with carbon numbers in excess of the parent hydrocarbon molecule are generated. Thus enlargements of the cyclic ring of methylcyclopentane leading to dibranched C_6 cyclic and aromatic molecules occur. This capability of zeolite β is of key importance for reforming since it can increase significantly the octane number of the feed stock. Similarly, zeolite β can enrich the cyclohexane with additional carbon atoms. The deactivation of the catalyst under the present operating conditions is probably due to the coke build up on its acid sites.

In contrast to the zeolite β, alumina does not promote either isomerization or enlargement of the feed molecules under the present conditions. This is due to the lower acidity and to the much larger pores it possesses. A combination of metal with both zeolite β and γ-Al_2O_3 may result in a bifunctional catalyst of value for reforming.

ACKNOWLEDGMENTS

The authors are indebted to professor C. R. F. Lund and to Mr. M. C. Hausladen and Mr. S. S. Peri for their valuable help in the H_2-Chemisorption experiments.

REFERENCES

1. Scherzer, J., "Catalytic Materials: Relation between Structure and Reactivity," ACS Symp., Vol. 248, p. 157. ACS, Washington, DC, 1984.
2. Wadlinger, R. L., Kerr, G. T., and Rosinski, E. J., U.S. Patent 3,308,069 (1967).
3. Wadlinger, R. L., Kerr, G. T., and Rosinski, E. J., U.S. Patent 3,308,064 (1975).
4. Newsam, J. M., Treacy, M. M. J., Koetsier, W. T., and DeGruyter, C. B., *Proc. R. Soc. London Ser. A* **420,** 375 (1988).
5. Treacy, M. M. J., and Newsam, J. M., *Nature* **332,** 249 (1988).
6. Higgins, J. B., LaPierre, R. B., Schlenker, J. L., Rohrman, A. C., Wood, J. D., Kerr, G. T., and Rohrbangh, W. J., *Zeolites* **8,** 446 (1988).
7. Camblor, M. A., and Perez-Pariente, J., *Zeolites* **11,** 202 (1991).
8. Perez-Pariente, J., Martens, J. A., and Jacobs, P. A., *Zeolites* **8,** 46 (1988).
9. Perez-Pariente, J., Martens, J. A., and Jacobs, P. A., *Appl. Catal.* **31,** 35 (1987).
10. Leu, L. J., Hou, Y. L., Kang, B. C., Li, C., Wu, S. T., and Wu, J. C., *Appl. Catal.* **69,** 49 (1991).
11. Lapierre, R. B., and Partridge, R. D., Eur. Pat. Appl. 94827 (1983).
12. Lapierre, R. B., Partridge, R. D., Chen, N. Y., and Wong, S. S., Eur. Pat. Appl. 95303 (1983).
13. Lapierre, R. B., Randell, D. P., Chen, N. Y., and Wong, S. S., U.S. Patent 4,501,926 (1985).
14. Martens, J. A., Perez-Pariente, J., and Jacobs, P. A., *in* "Chemical Reactions in Organic and Inorganic Constrained Systems" (E. Selton, Ed.) Kluwer, Dordrecht, 1986. NATO ASI Ser. C., Vol. 165, p. 115.
15. Corma, A., Fornes, V., Melo, P., and Perez-Pariente, J., *Prepr.-Am. Chem. Soc. Div. Pet. Chem.*, 632 (1987).
16. Corma, A., Fornes, V., Monton, J. B., and Orchilles, A. V., *J. Catal.* **107,** 288 (1987).
17. Ratnasamy, P. Bhat, R. N., Pokhriyal, S. K., Hegde, S. G., and Kumar, R., *J. Catal.* **119,** 65 (1989).
18. Wang, I., Tsai, T. C., and Huang, S. T., *Ind. Eng. Chem. Res.* **29,** 2005 (1990).
19. Weisz, P. B., *Adv. Catal.* **13,** 137 (1962).
20. Ciapetta, F. G., and Wallace, D. N., *Catal. Rev.* **5,** 67 (1971).
21. Ramage, M. P., Graziani, K. R., Schipper, P. H.,

Krambeck, F. J., and Choi, B. C., *Adv. Chem. Eng.* **13,** 193 (1987).
22. Satterfield, C. N., "Heterogeneous Catalysis in Industrial Practice," McGraw–Hill, New York, 1991.
23. Perez-Pariente, J., Sanz, J., Fornes, V., and Corma, A., *J. Catal.* **124,** 217 (1990).
24. Liu, S. B., Wu, J. F., Ma, L. J., Tsai, T. C., Wang, I., *J. Catal.* **132,** 432 (1991).
25. Yarlagadda, P., Lund, C. R. F., and Ruckenstein, E., *J. Catal.* **133,** 28 (1992).
26. Jacobs, P. A., and Martens, J. A., *in* "Synthesis of High-Silica Aluminosilicate Zeolites" (B. Delmon and J. T. Yates, Eds.), Vol. 33. Elsevier, Amsterdam, 1986.
27. Flanigen, E. M., *in* "Zeolite Chemistry and Catalysis" (J. A. Rabo, Ed.), ACS Monograph, ACS, Vol. 171, p. 80. Washington, DC, 1976.
28. Flanigen, E. M., Khatani, H., and Szymanski, H. A., *Adv. Chem. Ser.* **101,** 201 (1971).
29. Szostak, R., "Molecular Sieves: principles of Synthesis and identification," Van Nostrand–Reinhold Catalysis Series, New York, 1989.
30. Jacobs, P. A., Beyer, H. K., and Valyon, J., *Zeolites* **1,** 161 (1981).
31. Hegde, S. G., Kumar, R., Bhat, R. N., and Ratnasamy, P., *Zeolites* **9,** 231 (1989).
32. Babu, G. P., Hegde, S. G., Kulkarni, S. B., and Ratnasamy, P., *J. Catal.* **81,** 471 (1983).
33. Peri, J. B., *J. Phys. Chem.* **69,** 231 (1965).
34. Hindin, S. G., Weller, S. W., *J. Phys. Chem.* **60,** 1501 (1956).
35. Moretti, G., and Sachtler, W. M. H., *J. Catal.* **116,** 350 (1989).
36. Matsumoto, H., Saito, Y., and Yoneda, Y., *J. Catal.* **19,** 101 (1970).
37. Bolton, A. P., and Lanewala, M. A., *J. Catal.* **18,** 1 (1970).
38. Poutsma, M. L., and Schaffer, S. R., *in* "Zeolite Chemistry and Catalysis" (J. A. Rabo, Ed.), ACS Monograph, ACS, Vol. 171, p. 512. Washington, DC, 1976.
39. Scherzer, J., "Octane-Enhancing Zeolites FCC Catalysts." Dekker, New York, 1990.
40. Ciapetta, F. G., Dobres, R. M., and Baker, R. W., "Catalysis" (P. H. Emmett, Ed.), Vol. 6, p. 495. Reinhold, New York, 1958.
41. Sinfelt, J. H., Hurwitz, H., and Rohrer, J. C., *J. Phys. Chem.* **64,** 892 (1960).
42. Martens, J. A., Tielen, M., and Jacobs, P. A., *in* "Zeolites as Catalysts Sorbents and Detergent Builders" (H. G. Karge and J. Weitkamp, Eds.), Vol. 46, p. 49. Elsevier, Amsterdam, 1989.
43. Gault, F. G., *Adv. Catal.* **30,** 1 (1981).
44. Parera, J. M., Verderone, R. J., and Querini, C. A., *in* "Catalyst Deactivation" (B. Delmon and G. F. Froment Eds.), Vol. 34, p. 135. Elsevier, Amsterdam, 1987.
45. Kochloefl, K., and Bazant, V., *J. Catal.* **10,** 140 (1968).
46. Schulz, H., Weitkamp, J., and Eberth, H., *in* "Proceedings, 5th International Congress on Catalysis, Palm Beach, 1972" (J. W. Hightower, Ed.), Vol. 2, p. 1229. North-Holland, Amsterdam, 1973.
47. Weitkamp, J., Jacobs, P. A., Ernst, S., *in* "Structure and Reactivity of Modified Zeolites" (P. A. Jacobs, Ed.), Vol. 18, p. 279. Elsevier, Amsterdam, 1984.
48. Bolton, A. P., Lanewala, M. A., and Pickert, P. E., *J. Org. Chem.* **33,** 1513 (1968).
49. Sinfelt, J. H., and Rohrer, J. C., *J. Phys. Chem.* **65,** 978 (1961).
50. Venuto, P. B., Hamilton, L. A., Landis, P. S., *J. Catal.* **5,** 484 (1966).